EFFECTS OF SUPPORT STRUCTURE CHANGES ON FLOW-INDUCED VIBRATION CHARACTERISTICS OF STEAM GENERATOR TUBES

KI-WAHN RYU, CHI-YONG PARK[1] and HUINAM RHEE[2*]
Department of Aerospace Engineering, Chonbuk National University
664-14 Deokjin 1-Ga, Jeonju, Jeonbuk 561-756, Korea
[1] Korea Electric Power Research Institute
103-16 Munji-Dong Yuseong-Gu, Daejeon, 305-380, Korea
[2] School of Mechanical and Aerospace Engineering, Sunchon National University
413 Jungang-Ro, Sunchon, Jeonnam 540-742, Korea
[*]Corresponding author. E-mail : hnrhee@sunchon.ac.kr

Received March 5, 2009
Accepted for Publication August 4, 2009

Fluid-elastic instability and turbulence-induced vibration of steam generator U-tubes of a nuclear power plant are studied numerically to investigate the effect of design changes of support structures in the upper region of the tubes. Two steam generator models, Model *A* and Model *B*, are considered in this study. The main design features of both models are identical except for the conditions of vertical and horizontal support bars. The location and number of vertical and horizontal support bars at the middle of the U-bend region in Model *A* differs from that of Model *B*. The stability ratio and the amplitude of turbulence-induced vibration are calculated by a computer program based on the ASME code. The mode shape with a large modal displacement at the upper region of the U-tube is the key parameter related to the fretting wear between the tube and its support structures, such as vertical, horizontal, and diagonal support bars. Therefore, the location and the number of vertical and horizontal support bars have a great influence on the fretting wear mechanism. The variation in the stability ratios for each vibrational mode is compared with respect to Model *A* and Model *B*. Even though both models satisfy the design criteria, Model *A* shows substantial improvements over Model *B*, particularly in terms of having greater amplitude margins in the turbulence-excited vibration (especially at the inner region of the tube bundle) and better stability ratios for the fluid-elastic instability.

KEYWORDS : SG Tube, Support Structure, Fluid-elastic Instability (FEI), Stability Ratio, Turbulence Excitation (TE), Fretting Wear

1. INTRODUCTION

Flow-induced vibration, which is one of the main causes of tube defects, affects the top of the U-bend region of steam generator U-tubes of a nuclear power plant and leads to wear phenomena at contact points between the tube and its support structures, namely the diagonal, vertical, and horizontal support bars. To investigate the flow-induced vibration and wear mechanisms of steam generator tubes, many researchers have focused on fluid-elastic instability and turbulence excitation phenomena [1,2]. A fluid-elastic instability phenomenon provokes an excessive vibrational amplitude in the tube when the gap velocity exceeds the critical velocity. These excessive vibrations often lead to tube failure during a brief period of steam generator operation. Turbulence excitation can also cause fretting wear between a tube and its support structures, though the vibrational amplitude is relatively small. A well-designed steam generator is not affected by fluid-elastic instability but is subjected to small-amplitude vibrations that emanate from turbulence excitation [3]. As an example, the first tube failure occurred in 1971 and the second in 1997–twenty-six years after the initial start-up of the nuclear power station. This delay shows that fretting wear is a slow but continual damage mechanism [4]. That is, a long period of turbulence excitation can lead to a fretting wear problem.

Before 1980 little work had been done on the flow-induced vibration of tube bundles in a two-phase cross flow. Axisa *et al*. were the first to present results on the flow-induced vibration of a tube bundle subjected to both an air-water cross flow and a steam-water cross flow [5]. All tube bundles were subsequently tested in a two-phase flow with a void fraction of up to 99% [6-8]. Axisa *et al*.

carried out an extensive experimental program for various types of tube bundles and reported valuable results regarding the hydrodynamic mass, damping, fluid-elastic instability, and turbulence-induced excitation. Pettigrew and Taylor developed design guidelines to prevent failures due to excessive flow-induced vibration in shell-and-tube heat exchangers. Their study included an overview of the vibrational analysis procedures and recommended practical design guidelines [9,10]. Au-Yang *et al.* presented guidelines for the flow-induced vibration analysis of tubes and tube bundles, particularly those pertaining to steam generators, heat exchangers, condensers, and nuclear fuel bundles [1]. The guidelines were proposed as a nonmandatory code to be included in the ASME Code, Section III, Appendix N [2]. Thus, with regard to flow-induced vibration, the basic theories and guidelines proposed in previous studies are well developed [1-10]. However, a substantial amount of calculation is required to assess the integrity of steam generator tubes during the design stage and to determine the fluid-elastic instability and the response to turbulence excitation. For this purpose, we developed a computer program called Program for Integrity Assessment of a Steam Generator Tube (PIAT) [11]. PIAT, which processes thermal hydraulic data and performs a modal analysis and vibration response analysis very effectively, can efficiently handle all tubes of the steam generators in Korean nuclear power plants. It complies with the proven ASME code method, and its dynamic analysis of steam generator tubes has been validated [11].

Even though the steam generator has diagonal, vertical, and horizontal support bars at the U-bend region to prevent excessive amplitude due to the flow-induced vibration, wear defects on the tubes have often been reported for the previous version of the OPR1000 steam generators used at YGN 3&4 [12]. Eddy current tests have captured defective signals at contact points between the tubes and their support structures in the U-bend region. The defects mainly occur in the fretting wear zone, which is near the stay cylinder inside the steam generator (rows 25–40 and columns 64–102 of the YGN 3&4 steam generators) [12]. The fretting wear is strongly related to the magnitude of the flow velocity across the tube, the flow density around the tube, the unsteadiness of the flow, and the shape of the local vibrational mode at the supporting region of the U-tube. In-depth investigations have revealed two main causes of the wear phenomena at the central region of the steam generator: the high cross-flow velocity over the stay cylinder and the lack of adequate support conditions. The axial velocity over the stay cylinder can be reduced if an eggcrate flow distribution plate is installed in a revised steam generator model. As shown in Fig. 1(a) and Table 1, the revised design of Model *A* includes additional vertical and horizontal support bars in the middle of the steam generator to reinforce the support conditions. Model *B*, on the other hand, as shown in Fig. 1(b), does not have a vertical support bar in the middle of the U-tube; furthermore, in contrast with Model *A*, Model *B* has no horizontal strips below row number 41. Model *B* is based on the OPR1000 steam generator of the Korean standard nuclear power plant. Figure 2 shows enlarged views of the support structures of the two steam generator models. The U-tube consists of a vertical region above the tube sheet, a horizontal region at the top, and an arc region at the intersection of the horizontal and vertical parts.

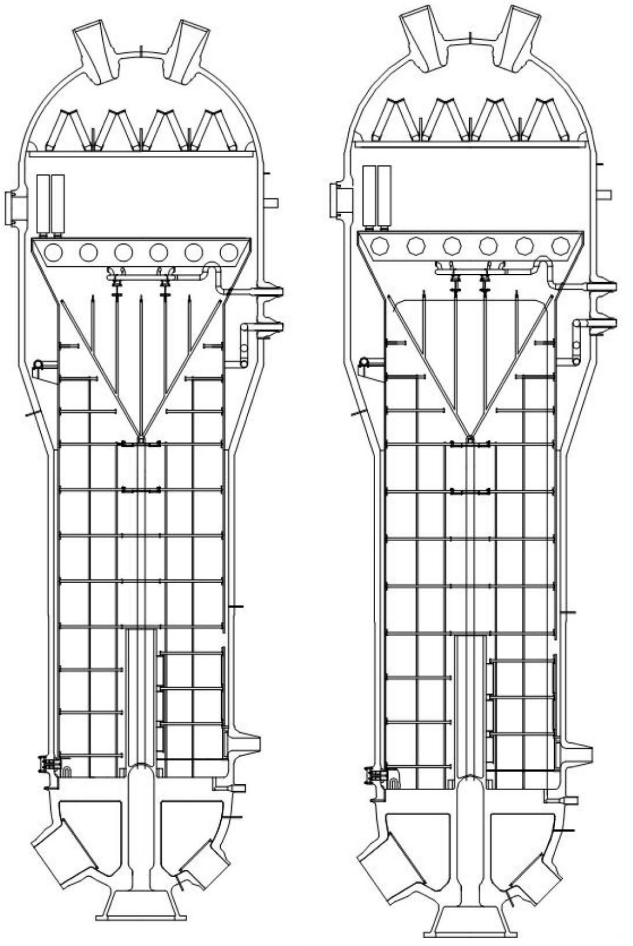

(a) SG Model *A* (b) SG Model *B*

Fig. 1. Configurations of the Steam Generator
(Courtesy of Doosan Heavy Industries and Construction)

Table 1. Design Parameter for Model Steam Generators

	SG Model *A*	SG Model *B*
Number of Vertical Support Bars	5	4
TSP Locations	Fig. 2 (a)	Fig. 2 (a)
Number of Tubes and Dimensions	Same	

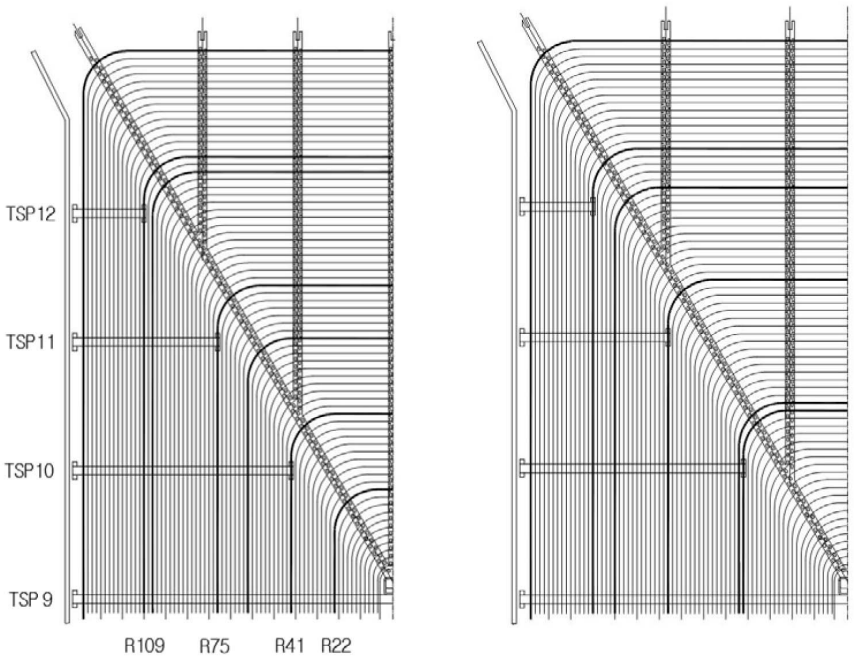

(a) SG Model *A* (b) SG Model *B*

Fig. 2. Configuration of the U-bend Region (Courtesy of Doosan Heavy Industries and Construction)

Because the mode shape acts as a weight function in response to flow-induced loads, the suppression of large modal displacements at the U-bend region is a key parameter for the safe design of steam generators. Through an intensive parametric study, we confirm that the support structures at the top of the U-bend region are strongly related to changing shapes of the different modes. Therefore, a comparison of Model *A* and Model *B* with regard to the two main parameters of flow-induced vibration, namely the stability ratios for the fluid-elastic instability and the amplitude of the vibration response to the turbulence excitation, confirms the effectiveness of the vertical and horizontal support bars. The PIAT code was used for all the necessary numerical computations in this study.

2. FLOW-INDUCED VIBRATION ANALYSIS OF STEAM GENERATOR TUBES

Figure 3 shows the overall procedure of the flow-induced vibration analysis. Each step is explained briefly in the following subsections.

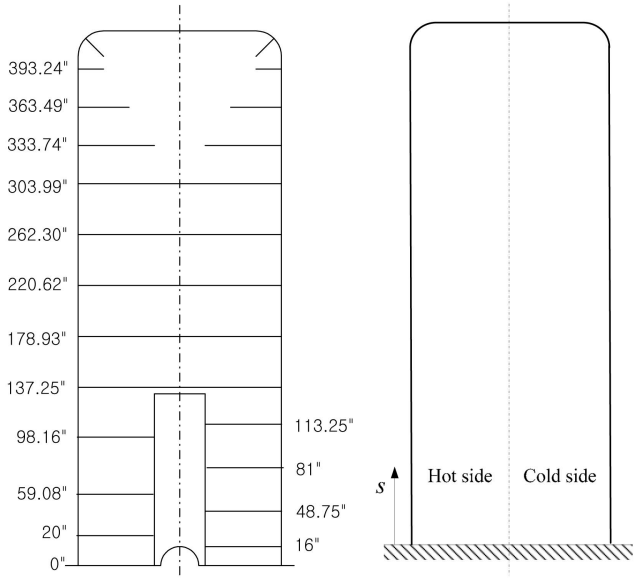

(a) TSP location (b) Tube coordinate *s*

Fig. 3. Schematic View of Tube Support Plates and Tube Coordinate System

2.1 Thermal-hydraulic Analysis

The thermal-hydraulic analysis of the inside the steam generator was conducted with the ATHOS3 code [13]. This code is a program that is commonly used to compute three-dimensional, two-phase, viscous thermal-hydraulic problems for several types of heat exchangers. The ATHOS3 code models tubes and internal structures by using a porous material concept; it also uses the experimental relations of heat and mass transfers. In the present analysis, the computational domain is bound between the upper side of the tube sheet and the bottom of the moisture separator

inside the shroud of the steam generator. The Neumann boundary conditions of mass, momentum, and energy flux on the tube sheet are applied. The feedwater mass flow rate and the temperature inside the steam generator are also applied to the inlet Dirichlet boundary condition. The outlet pressure is assumed to be a given dome pressure, and the flow conditions of the primary water, namely the pressure and temperature at the hot and cold legs and the mass flow rate, are all specified. All of these boundary conditions are set to be steady conditions at a full power level of 100%. Finally, our thermal hydraulic analysis of Model *B* is applied to both Model *A* and Model *B*.

2.2 Modal Analysis of U-tubes

The effective mass distribution per unit length along the steam generator tube can be determined with the following equation:

$$m(s) = m_t(s) + m_{pf}(s) + m_a(s), \tag{1}$$

where *s* is the spanwise coordinate along the tube from the hot side of the tube sheet to the cold side, as shown in Fig. 4(b), and *m* is the effective mass per unit length. The symbol m_t is the mass per unit length of the tube metal, m_{pf} is the mass per unit length of the primary water (coolant) inside the tube, and m_a is the added mass. These values vary along the tube. The added mass obtained from the fluid density outside the tube can be represented as follows [6]:

$$m_a(s) = c\rho(s)\frac{\pi d^2}{4}, \text{ where } c = \frac{(D_e/d)^2+1}{(D_e/d)^2-1} \tag{2a}$$

$$D_e/d = \begin{cases} (0.96+0.50p/d)p/d & \text{for triangular tube array} \\ (1.07+0.56p/d)p/d & \text{for rectangular tube array} \end{cases} \tag{2b}$$

where *c* represents the coefficient of added mass and ρ represents the two-phase mixture density at the shell side region. The symbol *p/d* denotes the pitch-to-diameter ratio of the tube array. Chen and Chung [14] also developed a computational code to obtain the added mass coefficient, though their results differ slightly from those of Eq. (2a). In this study, Eq. (2a) is adopted for convenience.

The modal analysis of the tubes in this study is performed with a specially designed computer program called the PIAT-MODE [15]. The program was developed to efficiently provide vibration characteristics of all the tubes. The different geometries, boundary conditions, fluid effects, and material properties of the tubes make the modal analysis of around 10,000 tubes physically impossible. As shown in Fig. 3, the PIAT-Mode acts as an intrinsic routine of the PIAT code. Clamped conditions are applied at the tube sheet and pin support conditions are applied at every tube support plate. All of the support conditions for the horizontal, vertical, and diagonal support bars are also considered [8]. Basically, the boundary condition along the tube axis is not restricted to a pinned-support condition. The diametral clearance between tube and its support structure is about 0.013" (0.33 mm). Actually scuffing is the most common support condition during flow-induced vibration. Thus, strictly speaking, the dynamic interaction is basically nonlinear, and the vibrational behavior of the U-tube is very complex because it simultaneously includes impact and sliding phenomena on the inside surface of the support. Most analysis programs for steam generator tubes, however, assume that there is a pinned support condition [9]. Most tubes with a typical span length of 1 m and a gap clearance of less than 0.33 mm make contact with the support structures, and we assume that the thickness of the support structures has a negligible effect on long span lengths such as the OPR1000 SG.

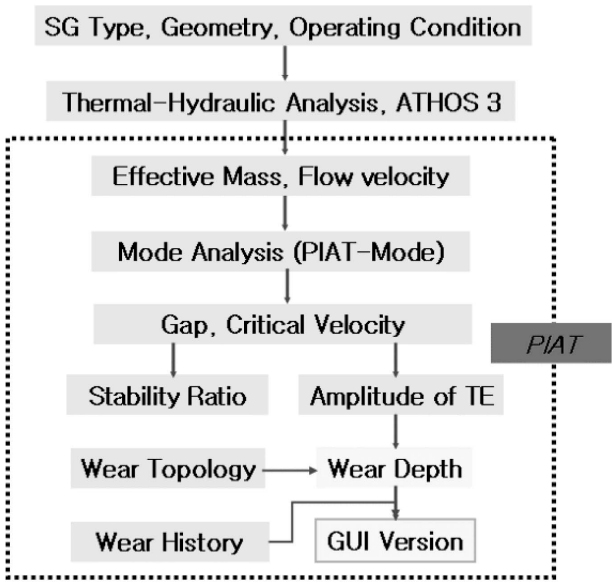

Fig. 4. Flow Chart for FIV and Wear Analysis of the PIAT Code

After the modal analysis, the natural frequencies and mode shapes of many modes must be input appropriately into the flow-induced vibration analysis module, as shown in Fig. 3. Because this process is arduous, we developed and implemented an algorithm that executes all these functions automatically; it also solves eigenvalue problems and constructs finite element models, as shown in the following equation:

$$\underline{M}\ddot{x} + \underline{K}x = 0\,. \tag{3}$$

where *M* denotes the mass and *K* denotes the stiffness matrix. The values of $\ddot{x}$ and *x* are the acceleration and displacement vectors, respectively.

2.3 Implementation of the Stability Ratio

In ordinary steam generators, the complex internal structure and three-dimensional flow produce the radial and axial components of the flow velocity, causing a no uniform flow around the steam generator tubes. When the Connors equation for nonuniform flow conditions is applied, the effective gap velocity for the *j*-th mode can be calculated as follows:

$$V_{ge,j}^{\ 2} = \frac{m_0}{\rho_0} \frac{\int_0^L \rho(s) V_g^{\ 2}(s) \phi_j^{\ 2}(s) ds}{\int_0^L m(s) \phi_j^{\ 2}(s) ds}, \tag{4}$$

where m_0_and ρ_0 are the reference values of the effective mass per unit length and flow density at the shell side, respectively; $\phi_j(s)$ and $V_g(s)$ denote the normalized mode shape of the *j*-th mode and the normal gap velocity for an array type of steam generator tube, respectively; and *L* represents the total length of the U-tube. The normal gap velocity can be obtained from the pitch velocity and the porosity ratio as follows:

$$V_g(s) = \alpha V_p(s) = (1-\beta)\frac{p}{p-d} V_n(s) \tag{5a}$$

$$\beta = \begin{cases} \pi d^2 / 2\sqrt{3} p^2 & \text{for triangular tube array} \\ \pi d^2 / 4 p^2 & \text{for rectangular tube array} \end{cases}, \tag{5b}$$

where *p* is the tube pitch and β is the porosity ratio obtained from cell-averaging. Equation (5b) can be derived from the concept of porosity. As shown in Fig. 5, the tube array types for the lower straight (vertical) region and the upper U-bend (horizontal) regions are of an equilateral triangular and diamond type, respectively. The reference values of the effective mass, m_0, and the flow density, ρ_0, are each weighted mean value properties along the entire tube length. They are expressed as follows:

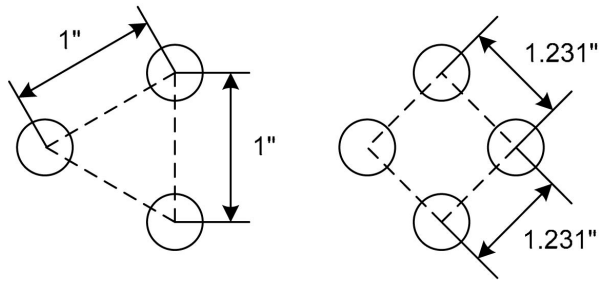

(a) lower (vertical) (b) upper (horizontal)

Fig. 5. Types of Tube Arrays for Model Steam Generators

$$m_0 = \frac{\int_0^L m(s)\phi_j^2(s) ds}{\int_0^L \phi_j^2(s) ds} \tag{6a}$$

$$\rho_0 = \frac{\int_0^L \rho(s)\phi_j^2(s) ds}{\int_0^L \phi_j^2(s) ds}. \tag{6b}$$

According to Chen [16] and Pettigrew and Gorman [17], many researchers have proposed a number of models and theories for estimating the critical velocity used in fluid-elastic instability analysis. Connors [18] was the first to experimentally investigate the fluid-elastic instability of tube bundles. From these results, the critical velocity for the *j*-th mode can be determined by using the following empirical equation:

$$V_{c,j} = K f_j d \sqrt{\frac{2\pi\zeta_j m_0}{\rho_0 d^2}}, \tag{7}$$

where f_j is the *j*-th natural frequency of the U-tube, ζ_j is the total damping ratio, and *K* represents the instability constant obtained from the available experimental results.

Many researchers have reported the coefficient of fluid-elastic instability, *K*, for several tube arrays [16-19]. Their research results indicate that the value of *K* is in the range of 2.4 to 9.9. Even though the array is of the same type, the values vary according to the experimental conditions, specifically the two-phase flow condition, the pitch-to-diameter ratio, the support conditions, and so forth. For the present analysis, the value of $K = 3.3$ was adopted from the available experimental data [2,7]. Most of the experiments in the two-phase flow condition were conducted with a *p/d* range of 1.4 to 1.5. For the OPR1000 steam generator, the *p/d* ratios are 1.33 for the vertical range and 1.64 for the horizontal region. The available 170 data points for the onset of instability [16] have a mean K value of 3.4 for a square array, 4.0 for a rotated triangular array, 4.5 for a triangular array, and 5.8 for a rotated square array [2]. There are no experimental data for a curved tube resembling the U-bend region. The OPR1000 steam generator has a rotated square tube array in the U-bend region. The stability ratio based on a recommended value of K = 3.3 [2,7] may have a greater margin for other tube arrays.

The overall damping ratio, which is in the range of 1%–5% or more, depends on the support and flow conditions [20]. For this study, we used an overall damping ratio of 1.5%, which covers the effects of viscous, support, and two-phase damping. This value was recommended by Au-Yang [1] for single and two-phase flow conditions with ideal support at both ends of a straight tube bundle.

The stability ratio for the *j*-th mode of the U-tube can

be defined by the ratio of $V_{ge,j}$ to $V_{c,j}$ as follows:

$$SR_j = \frac{V_{ge,j}}{V_{c,j}}. \tag{8}$$

The empirical results confirm that the vibrational amplitude increases intensely if the stability ratio exceeds a value of 1. This excessive amplitude can abruptly lead to wear or rupture of the tube. Therefore, the limit of stability ratios is set to a safe value of less than 1. The value of 0.75 is 0.33 mm generally used for the design of commercial steam generators [10].

2.4 Amplitude of Turbulence Excitation

Although turbulence excitation does not generate large vibrations, it is one of the main causes of the fretting wear that occurs at the contact points between the tube and its support structures over a long period of operation [3]. The vibrational amplitude of the tube due to the turbulence excitation can be calculated as follows in accordance with the ASME code (section III, appendix N) [2]:

$$\overline{y}_{rms} = \left\{ \sum_j \sum_i \frac{L_i G_i(f_j)[\varphi_j^2(s) + \phi_j^2(s)]}{64\pi^3 M_j^2 f_j^3 \zeta_j} (J_{jj}^i)^2 \right\}^{0.5}, \tag{9}$$

where J_{jj}^i denotes the joint acceptance of the j-th eigen mode at the i-th span [21,22]; the subscripts i and j denote the i-th span and the j-th eigen mode, respectively; and the symbols ϕ_j and φ_j denote the normal and tangential components of the mode shape function, respectively. The modal mass, M_j, the power spectral density due to random turbulence excitation, G_i, and J_{jj}^i can be expressed as follows:

$$M_j = \int_0^{L_i} m(s)[\phi_j^2(s) + \varphi_j^2(s)]ds \tag{10a}$$

$$G_i(f_j) = d^2 C_r^2(f_j) / 4 \int_0^{L_i} \{\rho(s) V_g^2(s) \phi_j(s)\}^2 ds \tag{10b}$$

$$(J_{jj}^i)^2 = \frac{\eta_i^2}{2 + (j\pi\eta_i)^2/2} \cdot \left[\frac{(j\pi\eta_i)^2 \{(-1)^{j+1} e^{-2/\eta_i} + 1\}}{2 + (j\pi\eta_i)^2/2} + \frac{2}{\eta_i} \right],$$

$$\text{where } \eta_i = \frac{l_c}{L_i} \tag{10c}$$

$$l_c = 0.4p(1 + p/2d). \tag{10d}$$

where l_c denotes the correlation length scale of turbulence [1]. The coefficient of random excitation, C_r, which is shown in the following equation, is based on Figure N-1343-1 of [2]:

$$C_r = \begin{cases} 0.025 & \text{for } 0 < f_j < 40 \text{ Hz} \\ 0.108 \times 10^{-0.0159 f_j} & \text{for } f_j \geq 40 \text{ Hz} \end{cases}. \tag{11}$$

Equation (11) determines the value of the random excitation coefficient for the upstream tube. The value in the interior of the tube bundle is half of that value. Equations (10b) and (11), which are valid for both horizontal and vertical tube sections, are based on the computed normal gap velocity.

According to WRC Bulletin No. 372 [23], which describes critical criteria for the design of steam generators, the amplitude of turbulence-induced vibration should be less than 10 mils to prevent damage due to fretting wear.

3. RESULTS AND DISCUSSION

Most signs of wear in steam generators that operate at Korean nuclear power plants are detected at contact points in the U-bend region of the steam generator tubes. It is therefore critical to reduce the local vibration mode at the uppermost region of the U-tube. This reduction decreases the stability ratio, the amplitude of turbulence excitation, and the possibility of fretting-wear in the U-bend region. Analysis of the flow-induced vibration problem requires interdisciplinary methods and ideas pertaining to thermal-hydraulic analysis, vibrational mode analysis, the concepts of fluid-elastic instability and turbulence excitation, wear mechanisms, and so on. Figure 3 shows the comprehensive procedure for analyzing flow-induced vibration. The thermal hydraulic data, such as the flow velocity, flow density, and void fraction, are obtained by using ATHOS3 code with computational fluid mechanics analysis. Table 2 lists the common operating data of steam generators Model *A* and Model *B*. The grid system adopted in this calculation is $20 \times 14 \times 43$ in the circumferential (θ), radial (r), and axial (z) directions, respectively. The

Table 2. Common Operating Data of the Model Steam Generators at Full Power

Parameter	Value
Dome pressure	1,070 psi
Primary water pressure	2,250 psi
Tube bend radius	10 inches
Tube outer diameter	0.75 inches
Tube thickness	0.04193 inches
Vertical pitch	1 inches
Horizontal pitch	1,231 inches
Young's modulus	27.85E6 psi
Tube material	Inconel 690

Table 3. Selected Tubes for Calculation

Designation	Row	Column	Remark
R12C109	12	109	near the stay cylinder
R22C105	22	105	near the stay cylinder
R37C97	37	97	near the stay cylinder
R41C84	41	84	longest span upper TSP 9 (Fig. 2)
R75C84	75	84	longest span upper TSP 10 (Fig. 2)
R109C84	109	84	longest span upper TSP 11 (Fig. 2)

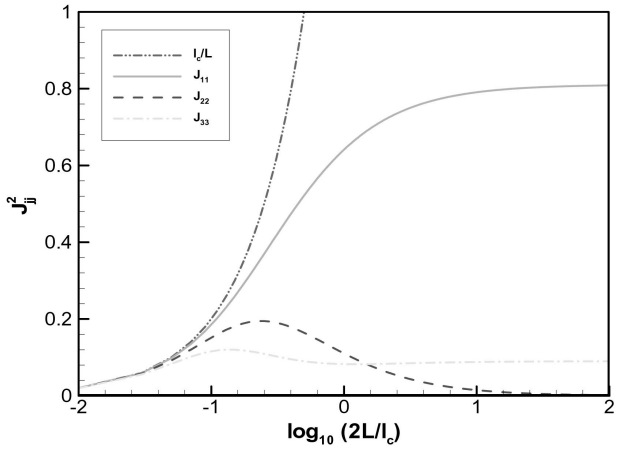

Fig. 6. Comparison of Joint Acceptance

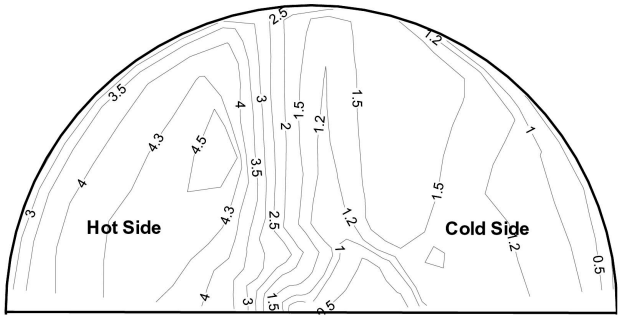

(a) Magnitude of flow velocity (m/sec)

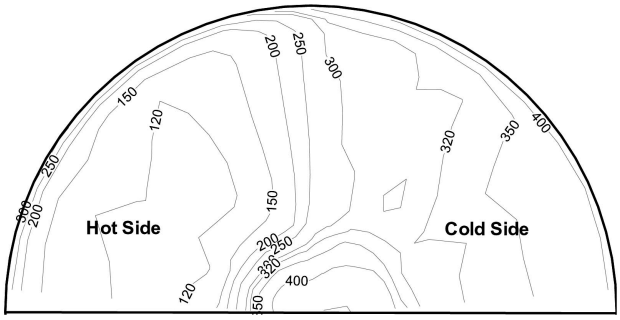

(b) Secondary flow density (kg/m^3)

Fig. 7. Flow Distribution at the Sectional Plane of SG (z = 8.25 m)

converged solution includes mixture velocity, mixture enthalpy, void fraction, mass quality, and water temperatures of the primary and secondary sides. From the thermal hydraulic data, the effective mass in Eq. (1) is obtained for modal analysis of the steam generator tube. The added mass effect of water adjacent to the U-tube is computed in Eqs. (2a) and (2b). As shown in Fig. 5, the tube arrays of the OPR1000 steam generator are of the triangular type in the vertical region and of the diamond (or rotated square) type in the horizontal region of the U-tube. From the schematic views of Fig. 5, the *p/d* ratios are 1.33 for the vertical region and 1.64 for the horizontal region. Finally, the stability ratio and the amplitude of turbulence excitation are calculated with Eqs. (8) and (9).

The six typical tubes used in this study are listed in Table 3 so that the stability ratio and the amplitude of turbulent excitation for Model *A* can be compared with the corresponding values of Model *B*. The R41C84 tube has a long tube support span around the U-bend region; note also, as shown in Fig. 4(a), that it belongs to a tube group that has 19 support positions between the tube and support plates. Of the tube groups that have the same support positions, the R75C84 and R109C84 tubes also have long tube support spans around the U-bend region. The R12C109, R22C105, and R37C97 tubes are located around the stay cylinder.

Figure 6 shows the square of joint acceptances: J_{11}^2, J_{22}^2, and J_{33}^2 versus $2L/l_c$ in Eq. (10c). These values may be approximated to l_c/L if $2L/l_c$ is small. However, in this study, we used exact values of the joint acceptances.

Figures 7(a) and 7(b) show the distributions of the flow velocity and the secondary side flow density at the axial location of 8.25 m from the tube support plate. The secondary flow density in the hot side region is lower than that in the cold side region. The recirculated inflow temperature on the tube sheet between the hot side region and the cold side region is nearly the same. However, due to the difference in heat transfer between the hot and cold sides, the secondary flow density in the hot side is lower. As shown in Fig. 7(a), this trend of lower density leads to the volumetric expansion and increases in the flow velocity.

Figure 8 plots the distribution of the effective mass and gap velocity along the tube coordinate s, from the bottom of the hot side to the bottom of the cold side, as shown in Fig. 3(b). The value of $s/s_0 = 0.5$ refers to the middle of the U-bend region. Due to the volumetric expansion, a region of small density and large flow speed develops at the hot side region. A high cross flow velocity therefore develops at the hot side of the U-bend region, potentially increasing the amplitude of the turbulence-

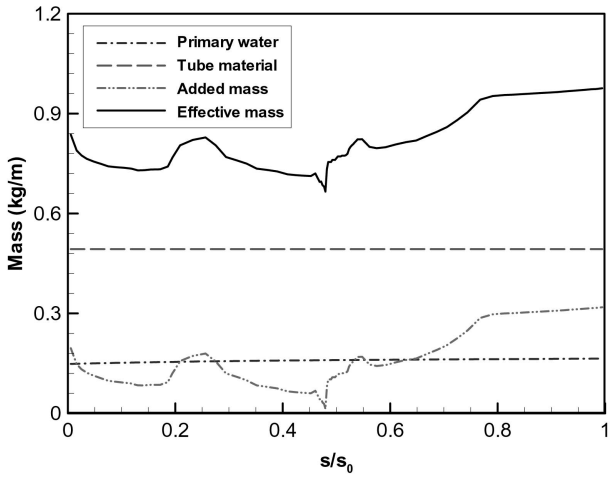

(a) Effective mass

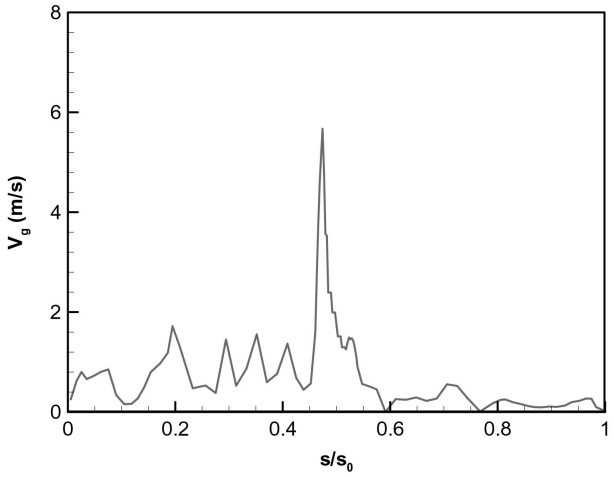

(b) Gap velocity

Fig. 8. Distribution of the Characteristics Value for R41C84

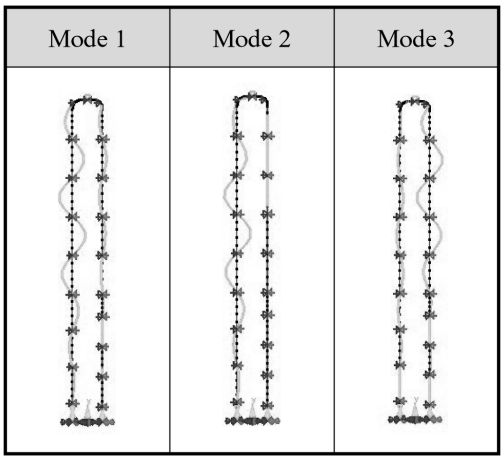

(a) SG Model *A*

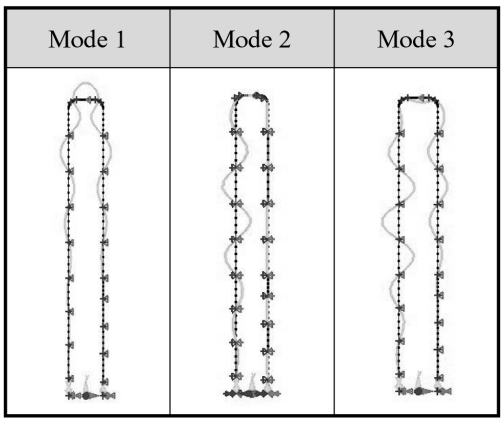

(b) SG Model *B*

Fig. 9. Mode Shapes of the R41C84 Steam Generator Tube

induced vibration.

Mode shapes were obtained by using the PIAT-Mode routine in the PIAT code. Figures 9(a) and 9(b) show the three lowest mode shapes of tube R41C84 (row number 41 and column number 84) of Model *A* and Model *B*. In Fig. 9, Model *B* displays the maximum modal displacement of its fundamental mode at the top of the U-bend region; Model *A*, on the other hand, displays little motion. This difference in mode shape may have a significant impact on the wear because the mode shape acts as a weighting function for important parameters such as the effective gap velocity in Eq. (4) and the amplitude of vibration in Eq. (9). Despite the high cross flow around the specified tube span, the vibration response may be small if the modal displacement is very small at the span. Therefore, as determined from a comparison of the mode shapes, Model *A* has better design features for reducing the flow-induced vibration responses. To validate the numerical

Table 4. Parameters of Three-span Tube Model

Descriptions		Value
Length	Span 1	36
	Span 2	35
	Span 3	46.375
Shell Side Fluid Density	Span 1	2.816E-6
	Span 2	2.771E-6
	Span 3	2.726E-6
Tube Side Fluid Density		6.352E-5
Outer Tube Diameter		0.625
Inner Tube Diameter		0.555
Young's Modulus of Tube Metal		2.9228E7
Density of Tube Metal		7.9257E-4
Damping Ratio		0.03
Natural Frequency		41.37

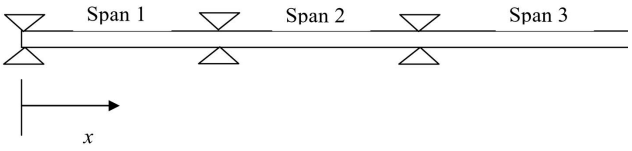

(a) Tube system

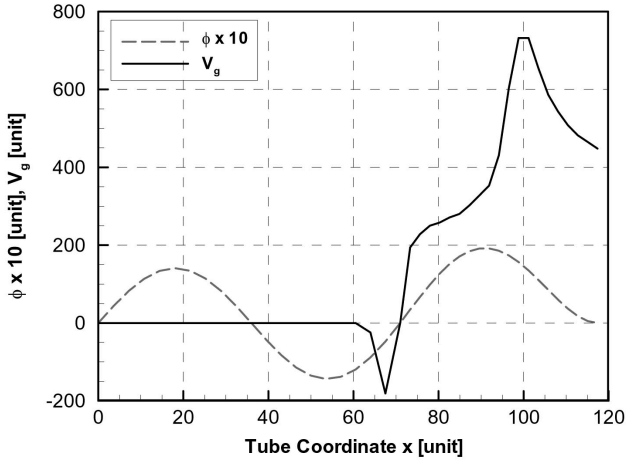

(b) Mode shape and cross flow velocity

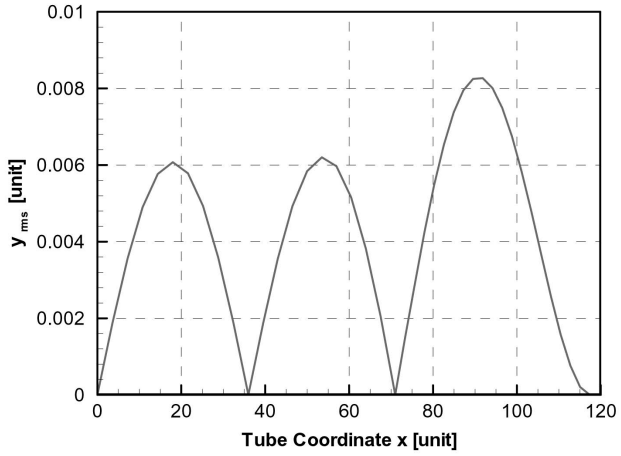

(c) Amplitude of turbulence excitation

Fig. 10. Validation of the Amplitude of Turbulence Excitation for Three-span Tube Model

procedure of the developed program, we compared the calculated results with those of the existing three-span tube problem [24]. Figure 10(a) shows the tube model clamped at the right end and simply supported at other three points. Table 4 lists the main parameters. Figure 10(b) plots the cross flow velocity, V_g, and the mode shape, ϕ, along the tube coordinate x. Figure 10(c) shows the amplitude of turbulence excitation along the tube span (as derived from Eq. (9)). The maximized amplitudes are located around the middle of each span. With this calculation, the developed program generates a maximum value of $\overline{y}_{rms}=8.3\times10^{-3}$ at the third span; in comparison with Au-Yang's result [24], our result has a relative error of only 1%.

Figures 11(a) to 11(f) show the amplitude of turbulence-induced vibration for the six selected tubes. The maximum amplitude of the tubes below row number 41 of Model *A* is reduced to between a third and a quarter of the corresponding value of Model *B*, while the amplitudes of the tubes above row number 41 are similar. This result means that the design change of the support structure, including the additional vertical and horizontal support bars in Model *A*, is beneficial, especially for the tubes near the stay cylinder, where the damage due to fretting wear has been reported. The amplitude of turbulence-induced vibration has an important effect on the fretting wear. Fretting wear damage can be estimated as follows by using Archard's formula:

$$\dot{V} = K\dot{W}\,, \tag{12}$$

where $\dot{V}$ is the material volume removal rate, K is the experimental fretting-wear coefficient, and $\dot{W}$ is the normal work rate. The normal work rate can be computed numerically from the following simplified expression [25]:

$$\dot{W} = 16\pi^3 f_j^3 mL\overline{y}_{\max}^2 \zeta_j\,. \tag{13}$$

Equations (12) and (13) show that the smaller amplitude due to turbulence excitation significantly reduces the wear. From Figs. 11(a) to 11(f), the maximum amplitudes of the turbulence excitation below row number 41 are drastically reduced by the additional vertical and horizontal support bars in Model *A*. Thus, the slight design modification of Model *A* greatly improves the wear characteristics.

Figures 12(a) to 12(f) show the stability ratios in relation to the vibrational modes for the six selected tubes. None of the stability ratios exceeds the design value of 0.75 [10]. Tube R41C84 shows a noticeable decrease in the stability ratios for Model *A*. This improvement is also due to the design change, including the additional vertical and horizontal support bars in Model *A*.

Although the original design of Model *B* meets the design criteria in terms of the stability ratio and the amplitude of the turbulence excitation, fretting wear still occurs in actual operating steam generator tubes. In many cases it is very difficult to clearly identify the causes of the wear because the integrity of the tubes can be affected by many other factors, such as as-built manufacturing and *in situ* operating conditions, contact topology, and some other unknown wear mechanisms beside the fluid-elastic instability and turbulence excitation. Regarding the flow-induced vibration, Model *A* is a better design because it provides more margins and therefore probably reduces the possibility of fretting wear problems due to flow-induced vibration.

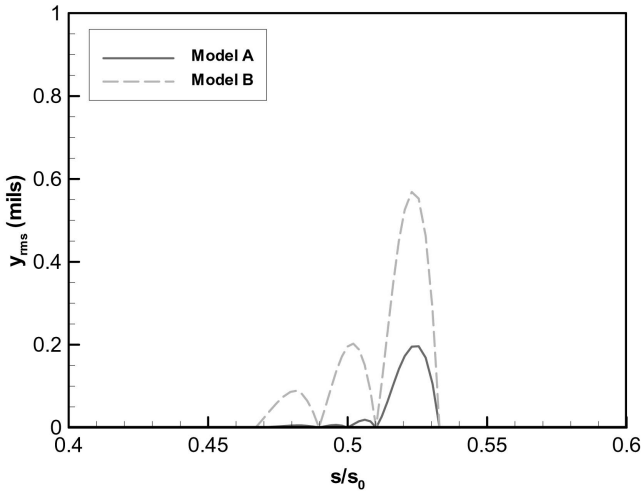

(a) R12C109

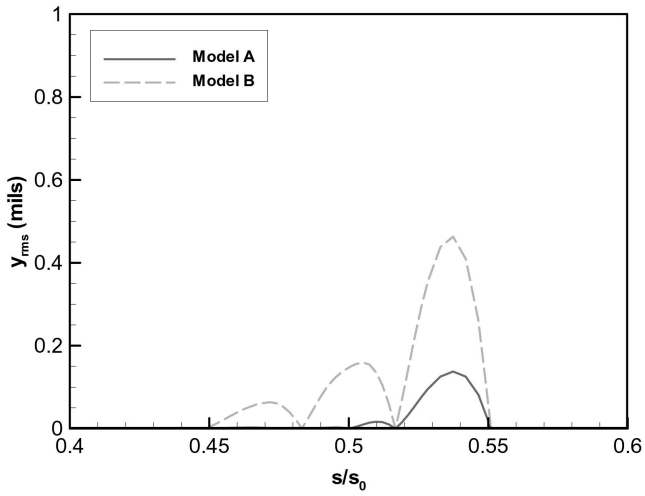

(b) R22C105

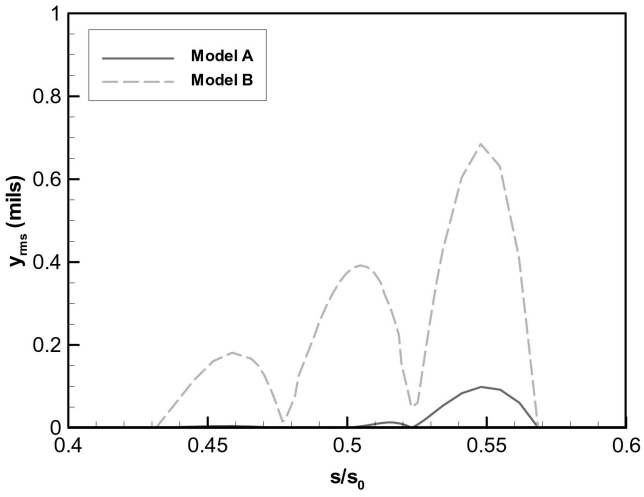

(c) R32C97

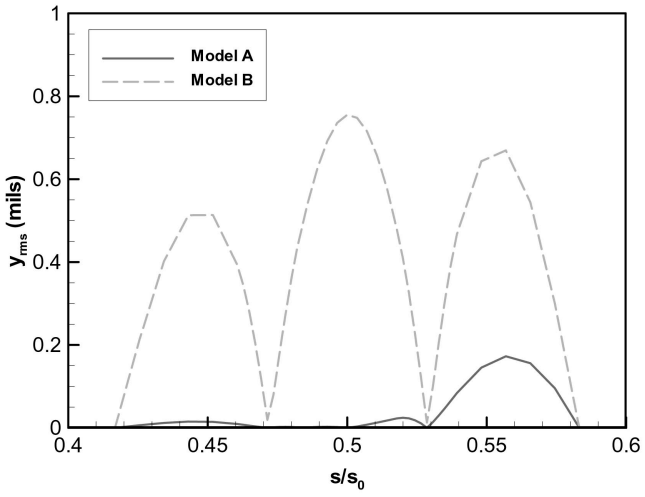

(d) R41C84

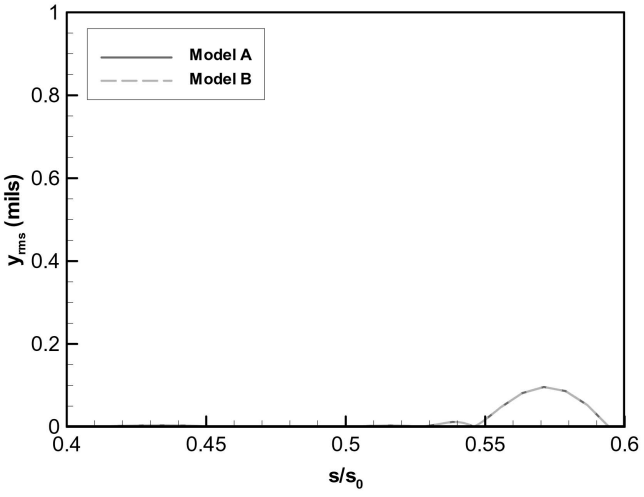

(e) R75C84

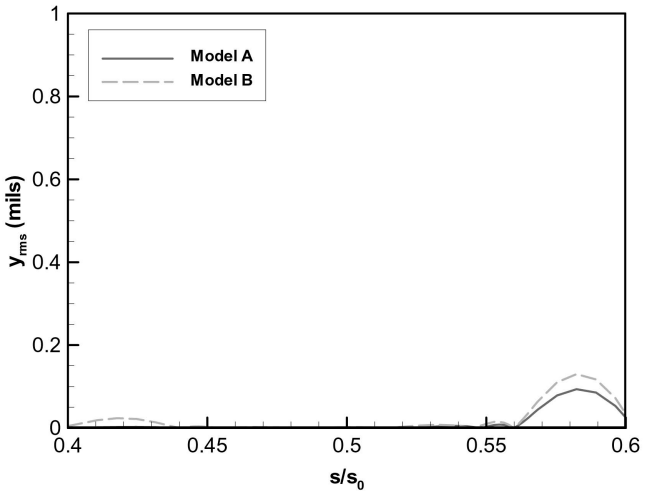

(f) R109C84

Fig. 11. Amplitudes of Turbulent Excitation for Various Tubes

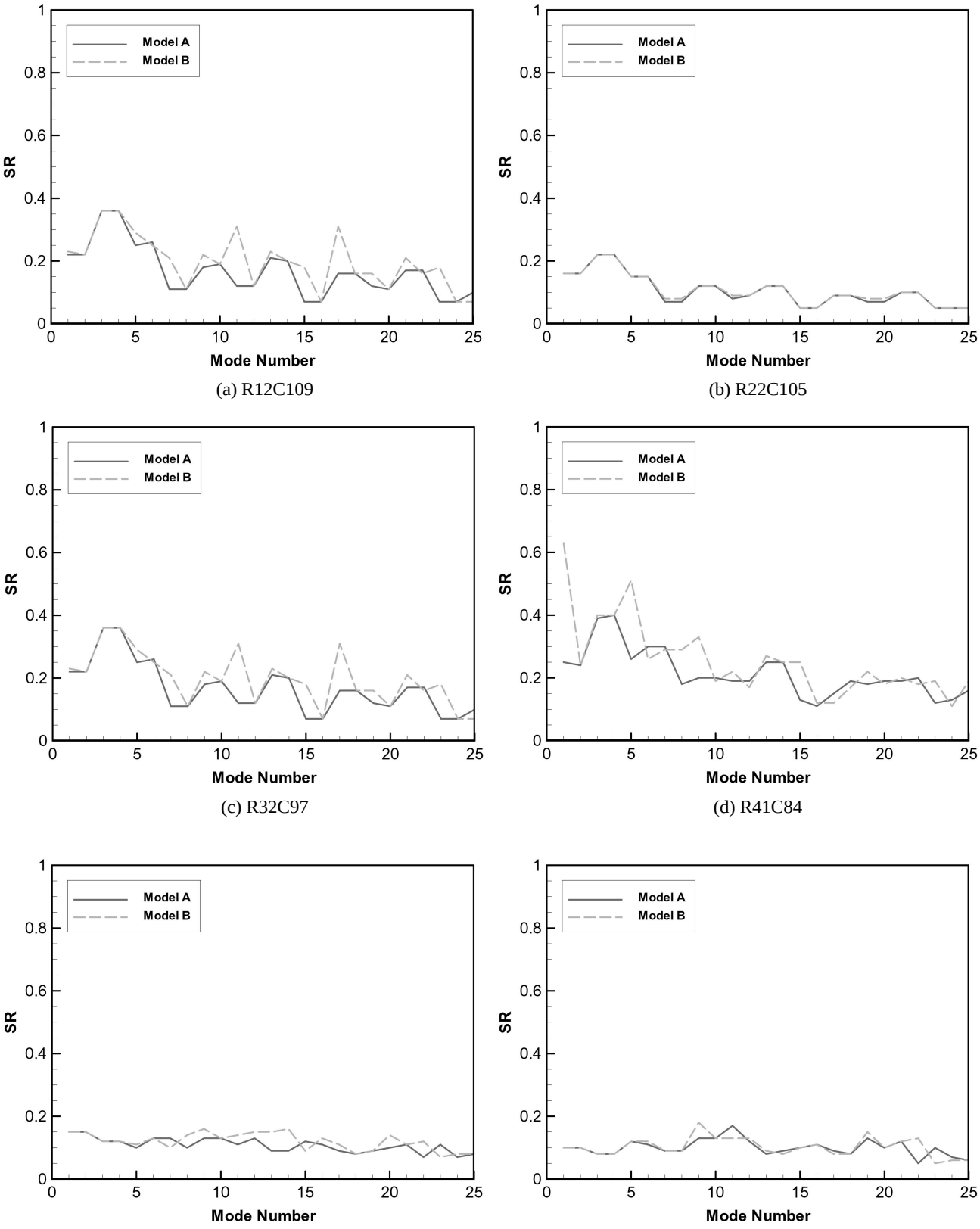

(a) R12C109 (b) R22C105

(c) R32C97 (d) R41C84

(e) R75C84 (f) R109C84

Fig. 12. Stability Ratios According to Vibrational Modes

4. CONCLUSION

A numerical study was performed to investigate how additional vertical and horizontal support bars in the U-bend region of a steam generator tube affect flow-induced vibration responses. Both the stability ratios regarding the fluid-elastic instability and the vibrational amplitudes due to the turbulence excitation were computed for the U-tubes of two steam generator models that are currently in use in nuclear power plants in Korea. The stability ratios and the amplitude of turbulence-induced vibration were then compared for Model *A* and Model *B*. The mode shapes and natural frequencies of Model *A* are different from those of Model *B*, mainly due to the change in the support structures with the insertion of additional vertical and horizontal support bars. This difference is especially apparent below row number 41. The maximum amplitude of vibration due to the turbulence excitation for Model *A* is decreased by a maximum of 75%. The maximum value of stability ratios of tubes in Model *A* is reduced to about 40%. Thus, the slight design modification of the support structures for the steam generator tubes can significantly improve the wear characteristics of the tubes.

ACKNOWLEDGEMENTS

This work was supported by KESRI (R-2007-2-052) and KESRI (2009T100100644), which is funded by MKE(the Korean Ministry of Knowledge Economy). The authors gratefully acknowledge the schematic drawing support of Doosan Heavy Industries and Construction.

REFERENCES

[1] M. K. Au-Yang, "Flow-Induced Vibration of Power and Process Plant Components, A Practical Workbook," ASME Press, (2001)

[2] ASME Code Section III, Rules for Construction of Nuclear Power Plant Components, Division 1 - Appendices, ASME Press, (1995)

[3] H. J. Connors, "Flow-Induced Vibration and Wear of Steam Generator Tubes," *Nuclear Technology*, Vol. 55, pp. 311-331 (1981)

[4] M. J. Pettigrew, L. N. Carlucci, C. E. Taylor, and N. J. Fisher, "Flow-Induced Vibration and Related Technologies in Nuclear Components," *Nuclear Engineering and Design*, Vol. 131, pp. 81~100 (1991)

[5] F. Axisa, B. Villard, R. J. Gilbert, G. Hetsroni, and P. Sundheimer, "Vibration of Tube Bundles Subjected to Air-Water and Steam-Water Cross-Flow: Preliminary Results on Fluidelastic Instability," *Proceedings of ASME Symposium on Flow-Induced Vibrations*, Vol. 2 pp. 269~284 (1984).

[6] M. J. Pettigrew, C. E. Taylor, and B. S. Kim, "Vibration of Tube Bundles in Two-Phase Cross-Flow: Part 1 – Hydrodynamic Mass and Damping," *J. of Pressure Vessel Technology*, Vol. 111, pp. 466-477 (1989)

[7] M. J. Pettigrew, J. H. Tromp, C. E. Taylor, and B. S. Kim, "Vibration of Tube Bundles in Two-Phase Cross-Flow: Part 2 – Fluid-Elastic Instability," *J. of Pressure Vessel Technology*, Vol. 111, pp. 478-487 (1989)

[8] C. E. Taylor, I. G. Currie, M. J. Pettigrew, and B. S. Kim, "Vibration of Tube Bundles in Two-Phase Cross-Flow: Part 3 – Turbulence-Induced Excitation," *J. of Pressure Vessel Technology*, Vol. 111, pp. 488-500 (1989)

[9] M. J. Pettigrew and C. E. Taylor, "Vibrational Analysis of Shell-and-Tube Heat Exchangers: an Overview – Part 1: Flow, Damping, Fluid-Elastic Instability," *J. of Fluids and Structures*, Vol. 18, pp. 469-483, (2003)

[10] M. J. Pettigrew and C. E. Taylor, "Vibrational Analysis of Shell-and-Tube Heat Exchangers: an Overview – Part 2: Vibration Response, Fretting Wear, Guidelines," *J. of Fluids and Structures*, Vol. 18, pp. 485-500, (2003)

[11] C. Y. Park, PIAT-GUI User's Manual, KEPRI, (2005)

[12] H. S. Jung, K. T. Kim, and H. D. Kim, "A Study on the Integrity Assessment of Defected SG Tube," TR.96NJ14. S2000.63, KEPRI, (2000)

[13] L. W. Keenton, A. K. Singhal, and G. S. Srikantiah, "ATHOS3 Mod-01: A Computer Program for Thermal-Hydraulic Analysis of Steam Generators," Vol. 1 ~ Vol. 4, EPRI NP-4604-CCML, (1990)

[14] S. S. Chen, and Ho Chung, "Design Guide for Calculating Hydrodynamic Mass Part I: Circular Cylindrical Structures," ANL-CT-75-45 (1976)

[15] H.N.Rhee, M.H. Boo, C.Y. Park and K.Y. Ryu, "Development and application of an efficient method for performing modal analysis of steam generator tubes in nuclear power plants", submitted to *Nuclear Eng. Design.*

[16] C. C. Chen, "Guidelines for the Instability Flow Velocity of Tube Arrays in Crossflow," *J. Sound and Vib.*, 93, pp. 439~455 (1984)

[17] M. J. Pettigrew, and D. J. Gorman, "Vibration of Heat Exchanger Tube Bundles in Liquid and Two-Phase Cross-Flow," Flow-Induced Vibration Design Guidelines, pp. 89~110.

[18] H. J. Connors, "Fluid-Elastic Vibration of Tube Arrays excited by Non-Uniform Cross Flow," Flow-Induced Vibration of Power Plant Components, *ASME J. of PVP*, 41, p. 93 (1980)

[19] H. J. Chung, and I. C. Chu, "Fluid-Elastic Instability of Rotated Square Tube Array in an Air-Water Two-Phase Cross-Flow," *Nuclear Engineering and Technology*, Vol. 38, pp. 69~80 (2006)

[20] J. C. Jo, and W. K. Shin, "Fluid-Elastic Instability Analysis of Operating Nuclear Steam Generator U-tubes," *Nuclear Eng. Design*, Vol. 193, Issues 1-2, pp. 55~71 (1999)

[21] M. K. Au-Yang, "Joint and Cross Acceptances for Cross Flow-Induced Vibration Part I – Theoretical and Finite-Element Formulations," PVP Vol. 389 pp. 17~24 (1999)

[22] M. K. Au-Yang, "Joint and Cross Acceptances for Cross Flow-Induced Vibration Part II – Charts and Applications," PVP Vol. 389 pp. 25~33 (1999)

[23] J. B. Sandifer, "Guidelines for Flow-Induced Vibration Prevention in Heat Exchangers," WRC Bulletin No. 372, (1992)

[24] M. K. Au-Yang "Turbulent Buffeting of a Multispan Tube Bundle," *Transactions of the ASME, J. of Vibration, Acoustics, Stress, and Reliability in Design*, Vol. 108, pp. 150~154 (1986)

[25] M. Yetisir, E. McKerrow, M. J. Pettigrew, "Fretting Wear Damage of Heat Exchanger Tubes: a Proposal Criterion based on Tube Vibration Response," *ASME J. of Pressure Vessel technology*, Vol. 120, pp. 297~305 (1998)